

# Pix2Prof: fast extraction of sequential information from galaxy imagery via a deep natural language ‘captioning’ model

Michael J. Smith,<sup>1,2,3\*</sup> Nikhil Arora,<sup>3</sup> Connor Stone,<sup>3</sup> Stéphane Courteau,<sup>3</sup> and James E. Geach<sup>1,2</sup>

<sup>1</sup>Centre for Astrophysics Research, Department of Physics, Astronomy & Mathematics, University of Hertfordshire, Hatfield, AL10 9AB, UK

<sup>2</sup>Centre of Data Innovation Research, Department of Physics, Astronomy & Mathematics, University of Hertfordshire, Hatfield, AL10 9AB, UK

<sup>3</sup>Department of Physics, Engineering Physics & Astronomy, Queen’s University, Kingston, ON, K7L 3N6, Canada

29 April 2021

## ABSTRACT

We present ‘Pix2Prof’, a deep learning model that can eliminate any manual steps taken when extracting galaxy profiles. We argue that a galaxy profile of any sort is conceptually similar to a natural language image caption. This idea allows us to leverage image captioning methods from the field of natural language processing, and so we design Pix2Prof as a float sequence ‘captioning’ model suitable for galaxy profile inference. We demonstrate the technique by approximating a galaxy surface brightness (SB) profile fitting method that contains several manual steps. Pix2Prof processes  $\sim 1$  image per second on an Intel Xeon E5-2650 v3 CPU, improving on the speed of the manual interactive method by more than two orders of magnitude. Crucially, Pix2Prof requires no manual interaction, and since galaxy profile estimation is an embarrassingly parallel problem, we can further increase the throughput by running many Pix2Prof instances simultaneously. In perspective, Pix2Prof would take under an hour to infer profiles for  $10^5$  galaxies on a single NVIDIA DGX-2 system. A single human expert would take approximately two years to complete the same task. Automated methodology such as this will accelerate the analysis of the next generation of large area sky surveys expected to yield hundreds of millions of targets. In such instances, all manual approaches – even those involving a large number of experts – will be impractical.

**Key words:** methods: data analysis – methods: statistical – galaxies: photometry.

## 1 INTRODUCTION

Large astrophysical surveys such as the Sloan Digital Sky Survey (SDSS; York et al. 2000), the Panoramic Survey Telescope and Rapid Response System (Pan-STARRS; Chambers et al. 2016), the Hyper Suprime Cam (HSC; Aihara et al. 2017) Subaru Strategic Program Survey, or the upcoming Vera C. Rubin Observatory Legacy Survey of Space and Time (LSST; Ivezić et al. 2019), carry an inherent scaling problem. The SDSS has observed over 35 per cent of the sky, cataloguing over 1 billion astronomical objects (Ahumada et al. 2020) with a data rate of raw multiband imagery approaching 200 GB per night. In January 2019, Pan-STARRS second Data Release totalled 1.6 PB of imaging data. A precursor to LSST, HSC’s 990 megapixel camera has already produced over 1 PB of imaging data (Aihara et al. 2019). These surveys will be dwarfed by the upcoming LSST project. LSST’s 3.2 gigapixel camera will be the largest ever made, and will survey the entire visible sky twice per week, generating  $\sim 500$  PB of imaging data over its decade-long mission. The ‘firehose’ of data from surveys such as LSST will require correspondingly efficient and fully automated procedures to curate and analyse the data, enabling new astrophysical findings and making unanticipated discoveries.

In this study, we are concerned with the automated direct analysis of galaxy imagery towards estimating galaxy properties such as size, luminosity, colour, and stellar mass. To calculate these properties,

one typically applies a photometric analysis that involves extracting and characterising the spatial distribution of a galaxy’s light, described by a surface brightness (SB) profile. The galaxy structural parameters as reflected by the SB profile can be used to infer a suite of other important characteristics such as light concentration, age, star formation rate, and assembly history (e.g. Strom et al. 1976; Bell et al. 2003; Shen et al. 2003; Bernardi et al. 2005; Fernández Lorenzo et al. 2013; Trujillo et al. 2020).

Numerous catalogues of galaxy structural properties already exist (Jedrzejewski 1987; Courteau 1996; Brinchmann et al. 2004; Blanton et al. 2005; Hall et al. 2012; Gilhuly & Courteau 2018). Unfortunately, the methods used in these compilations are either time consuming, requiring human supervision, or fast but unreliable since they require *a priori* assumptions about the shapes of galaxy components and other features. Similarly to the study detailed in this paper, Tuccillo et al. (2018) describe a fully automated neural network based technique (named ‘DeepLeGATo’; Deep Learning Galaxy Analysis Tool) designed to replicate the GALFIT model-dependent algorithm. DeepLeGATo is a fine example of an effective application of deep learning, providing faster and possibly more accurate analysis than its parent method, GALFIT (Peng et al. 2002). However, DeepLeGATo inherits from its similarity to GALFIT the same issues stated previously; namely, the hard-coded assumption of galaxy profile shapes, and other features. Furthermore, DeepLeGATo can only produce single float outputs, and so cannot infer an SB profile directly. This means that DeepLeGATo must rely on an

\* E-mail: m.smith28@herts.ac.uk

intermediary model to generate a complete SB profile. Therefore, even with semi-automated methods, the accurate extraction of *all* the useful information from existing surveys would take years. With the data volume expected to grow significantly in the coming years, this becomes an intractable problem. Of great concern is the possibility that important discoveries and insight could be missed or delayed significantly due to the technical challenges imposed by the unprecedented data volume. Clearly, there is a pressing need for entirely new and efficient automated methods that significantly reduce, and ideally circumvent, human interactions. Machine learning is ideally suited for this task, and we apply it in this paper towards the specific problem of extracting SB profiles from multi-band imaging data. Our approach takes advantage of a set of SB profiles already determined via classical, interactive methods (Courteau 1996; Gilhuly & Courteau 2018). We describe the classical method used to produce the training data set in the next section. The remainder of the paper is organised as follows: Section 2 introduces our approach; our results and validation are presented in Section 3; Section 4 addresses our global findings, and concludes with suggestions for broader application of the algorithm.

## 2 METHOD

### 2.1 The classical surface brightness profile extraction algorithm

In the surface photometry of galaxies (e.g. Courteau 1996, and references therein), the spatially resolved light profile of a galaxy is extracted by fitting progressively larger isophotes about a common centre. The fitting technique assumes that projected isophotes are well represented by ellipses. A galaxy’s centre is found by identifying the brightest pixel in a manually selected region. Given a manually defined galaxy centre, the classical algorithm determines the parameters needed to define each ellipse via a least squares optimisation. The algorithm then generates isophotal solutions at each radius well into the faint outskirts of the galaxy. In these regions of lower signal-to-noise, where fitting algorithms are challenged, the algorithm radially extends the last fitted isophote in the previous operation with a set of concentric isophotes out to an arbitrarily large radius, usually taken to be the edge of the image.

The isophotes may vary in ellipticity and position angle as a function of galactocentric radius. This can become problematic when fitting to non-axisymmetric structures in galaxies, such as bars and spiral arms that can cause large twists in the fitted isophotal map. This issue can be corrected by manually applying a smoothing function to some portions of the image. The latter consists of manually smoothing the contour fits (i.e. uncrossing twisted isophotes), and replacing poorly fitted data with a polynomial smoothing function. Note that, prior to applying isophotal fitting to galaxy images, some pre-processing is also required: the galaxy centre must be identified as described above; the ‘sky’ background must be estimated and removed from the image; nuisance foreground objects (such as unassociated galaxies or foreground stars) must be identified and masked. These steps add to the manual supervision of the task.

Besides the assumption that galaxies are circular when viewed face-on, and thus generally of elliptical appearance when projected on to the plane of the sky, the algorithm purposefully avoids using *a priori* knowledge of galactic disc profile shapes and other features such as bars, rings, and spiral arms. This avoids biasing the isophotal solution to any pre-determined, and possibly incorrect, shape – a problem especially acute in the faint outer edges of a galaxy.

While the semi-automated steps outlined above yield high quality

**Table 1.** A summary of the Courteau (1996) surface brightness profile fitting algorithm’s processes. An approximate wall time per galaxy is given for the manual sections. The automated sections’ time contributions are negligible.

| Process                          | Automated? | Wall time (s/gal) |
|----------------------------------|------------|-------------------|
| Identify galaxy centre           | No         | 5                 |
| Estimate & remove sky background | Yes        | –                 |
| Remove foreground objects        | No         | 120               |
| Fit contours                     | Yes        | –                 |
| Extend contours to galaxy extent | No         | 30                |
| Smooth isophotes                 | Yes        | –                 |
| Interpolate poorly fitted data   | No         | 120               |

SB profiles, the process of obtaining a single profile is slow and systematic variations may exist between different profile extraction methods. The interactive nature of certain steps may indeed give rise to marked profile differences, especially in low SB regimes where the isophotal solutions are less robust. The low SB regimes will always remain the bane of galaxy image analysis, whether automated or interactive, but the elimination of subjective steps goes a long way towards reducing systematic differences between profiles. Therefore, it becomes desirable to eliminate all interactive steps while retaining all the benefits of classic algorithms such as Courteau (1996) described above. In this work, we present a fully automated solution that incorporates the extant knowledge base of SB profile fitting methodology, but avoids human interaction.

### 2.2 Borrowing from automated image captioning

In recent years, the field of automated image captioning has benefited greatly from advances in deep learning. We were strongly influenced by these developments when designing the architecture of our ‘Pix2Prof’ profile estimator. In this section, we briefly review pure recurrent neural network (RNN) based encoder–decoder architectures, or models that only use a single encoder and decoder to generate captions. A comprehensive review on deep learning methods applied to image captioning can be found in Hossain et al. (2019).

We primarily draw inspiration from gated RNN based encoder–decoder architectures, as seen in Sutskever et al. (2014) for sequence-to-sequence translation, and in Vinyals et al. (2015), Jia et al. (2015), and Wang et al. (2016) for image-to-sequence translation. Sutskever et al. (2014) uses a Long Short Term Memory (LSTM; Hochreiter & Schmidhuber 1997) network to encode a given sentence to a latent descriptive vector, and a second LSTM network to decode the descriptive vector into a different feature space. One can use this technique to translate text between two different languages, for example.

Vinyals et al. (2015), Jia et al. (2015), and Wang et al. (2016) all use a convolutional neural network (CNN; Fukushima 1980; LeCun et al. 1989) to first encode an image to a latent descriptive vector, and then use an LSTM network to decode this vector into a text description (caption) of a given image. Xu et al. (2015) use a CNN encoder, and a LSTM that attends over the CNN output. Attention allows this approach to link each word in the caption with an associated part of the image. This approach works well for images that are crowded with multiple objects, but a simpler approach is preferred for our case where each image is dominated by a single, central galaxy.

A galaxy profile can be thought of as analogous to a text caption describing that galaxy. Both a text caption and galaxy profile can be encoded as a list of floats or integers, and both have a length and content dependent on the context of the conditioning image. Both also

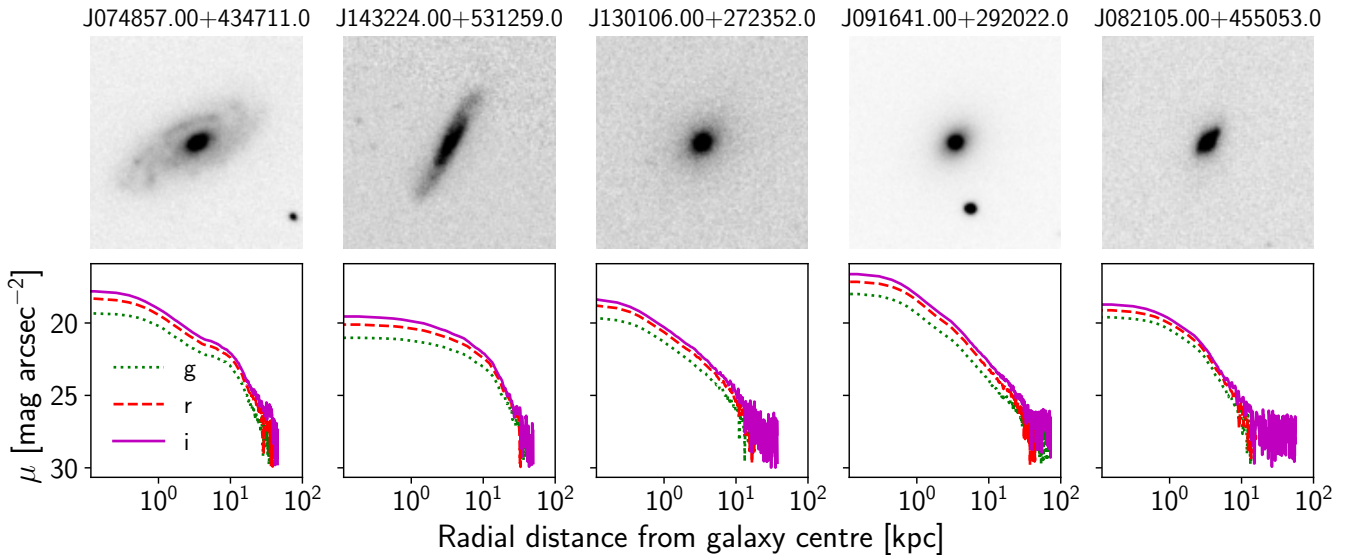


**Figure 1.** SDSS images of sample galaxies in the  $g$  band (top row), and corresponding surface brightness ‘ground truth’ profiles (bottom row).  $\mu$  is the surface brightness. The galaxy names above each image refer to their J2000 celestial coordinate.

need to terminate once a complete sentence or profile is generated, a subjective task well suited to a machine learning solution. RNNs learn where to terminate a given caption or profile empirically from the training set. Additionally, galaxy profiles and text captions can both be approximated with an appropriate RNN. RNNs also produce spatially consistent captions as a consequence of the architecture, a property not guaranteed in a straight one-shot CNN. With these benefits in mind, it is natural to consider an encoder–decoder network for the specific task of estimating challenging galaxy profiles. Importantly, since the proposed model directly learns the transformation between an unprocessed galaxy image, and the galaxy’s corresponding SB profile, it eliminates all of the manual steps described in Section 2.1 and Table 1.

While we develop Pix2Prof within the context of galaxy SB profile extraction, the model is equally applicable to any array  $\rightarrow$  float sequence translation task.

### 2.3 Training set

We initially populate our data set with  $10 \text{ arcmin} \times 10 \text{ arcmin}$   $g$ ,  $r$ , and  $i$  band image crops extracted via the SDSS DR10 (York et al. 2000; Eisenstein et al. 2011; Ahn et al. 2014) online mosaic interface. Each image is centred on a galaxy. From these images we extract an SB profile via the method described in Section 2.1. Fig. 1 presents a random sample of training set galaxies, and their corresponding, manually extracted SB profiles. The 1953 galaxy image–SB profile pairs in each of the  $g$ ,  $r$ , and  $i$  bands yield a total of 5859 pairs. This full data set is then divided into training, validation, and testing sets. There are 5367 galaxy image–profile pairs in the training set, 192 galaxy image–profile pairs in the validation set, and 300 galaxy image–profile pairs in the test set. The sets are randomly assigned, with the condition that a given galaxy’s three photometric bands are kept within the same set. The subset sizes are chosen to maximise the training set efficacy while retaining most of the training set variance in the test set.

The only destructive pre-processing performed on the galaxy imagery is a 99.9th percentile clipping. This clipping mitigates the issue of single bright (i.e. ‘hot’) pixels reducing image contrast when the

galaxy images are normalised, which would reduce training efficacy. To this end, we apply a fixed min-max normalisation, defined as

$$\bar{x} = \frac{x - A}{B - A}, \quad (1)$$

where  $A = 2.0$  nanomaggies is the floor of the minimum value in the training set, and  $B = 30.0$  nanomaggies is the ceiling of the 99.9th percentile value in the training set.

To reduce information sparsity in the training set images, we further crop each galaxy image to a shape of  $[256, 256]$  pixels before passing the image to Pix2Prof. We train using the full 32-bit depth of the original data as measured. Good quality data are paramount when training a neural network, and we therefore cut the profiles when the signal-to-noise ratio reaches a quality threshold. We terminate the profile when the signal-to-noise ratio of a 1D convolution with a length of 40 pixels ( $= 8 \text{ arcsec}$ ) reaches a threshold of 4. We define signal-to-noise so that it is equivalent to the ratio of the power of a signal to the power of background noise:  $(\mu/\sigma)^2$ , where  $\mu$  is the mean and  $\sigma$  is the standard deviation of the convolutional window.

### 2.4 Network architecture

We write our model in PyTorch (Paszke et al. 2019), using a ResNet-18 (Srivastava et al. 2015; He et al. 2016) encoder, and a Gated Recurrent Unit (GRU; Cho et al. 2014) decoder architecture. This architecture takes an arbitrarily sized single channel image input, and outputs a sequence of floats of arbitrary length. These floats are spaced along a galaxy’s semimajor axis at a spacing of  $0.2 \text{ arcsec}$  per step (the same as the Courteau (1996) technique). The same network is trained on images in the  $g$ ,  $r$ , and  $i$  bands, and therefore can produce a SB profile in any one of these bands. Fig. 2 shows a representation of the architecture used.

We use the standard ResNet-18 architecture as described in He et al. (2016). The GRU is stacked to three layers. We apply a rectified linear unit (Glorot et al. 2011, ReLU) activation and a dense neural layer after the three layer stack to reduce the number of output values to one. As a regularising measure, we apply dropout at a 20 per cent rate (Srivastava et al. 2014). The ResNet first encodes the incoming

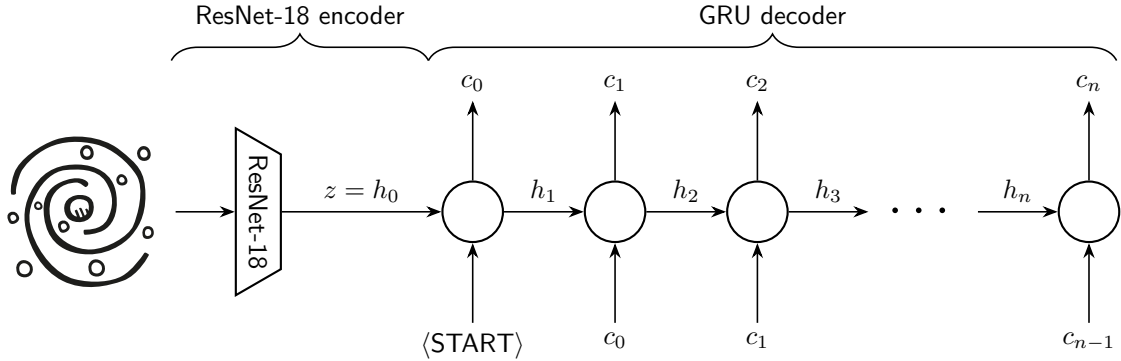


**Figure 2.** The ResNet → GRU encoder–decoder architecture used in this work. The hidden state  $h_i$  is the internal state of the GRU, and is dependent on both the galaxy latent encoding  $z$ , and the previous profile predictions  $c_i$ .

galaxy image to a latent space vector  $z$  of length 512. This vector is then used as the initial hidden state  $h_0$  of a GRU. In this way, Pix2Prof encodes and passes relevant information from the image to the GRU. The GRU then unrolls to estimate properties of the galaxy from  $z$ . In this paper’s case, we demonstrate this process by using  $z$  to estimate a galaxy’s SB profile.

To start estimation, the GRU is fed a start of sequence token. This token is set as an array of zeros. In place of an end of sequence token, the GRU is programmed to halt after 100 predictions are output that have a standard deviation of 0.01 or less. This ensures that the GRU halts estimation once it encounters the background sky.

We use the Adam optimiser (Kingma & Ba 2014) to train Pix2Prof via gradient descent (Robbins & Monro 1951). Using manual search, we set the learning rate as  $2 \times 10^{-4}$ . Due to the logarithmic nature of magnitude, we want to penalise large deviations from our ground truth SB profiles at a higher rate compared to small deviations, and so we use the mean squared error loss:

$$\text{MSE} = \frac{1}{b} \sum_{i=1}^b (y_i - p_i)^2, \quad (2)$$

where  $b$  is the batch size,  $y$  is the ground truth, and  $p$  is a prediction.

## 2.5 Training the model

We augment the galaxy images by applying a ‘wobble’. This wobble is a random small shift in the centre of the image. Each band is treated independently. We do this to encourage the network to work with the slightly off-centre galaxies that will be encountered in real data. This is required to make Pix2Prof robust to poorly centred galaxy images. We also exploit the rotational axisymmetry of galaxies and further augment the data by randomly rotating an input image through 90, 180, and 270 degrees.

We train the model for 100 000 global steps on a single NVIDIA TESLA V100 GPU. Training takes approximately 20 minutes per epoch of 500 galaxy images, a rate of 0.4 galaxies per second.

## 3 RESULTS & VALIDATION

We validate the model during training once per epoch using the validation set. We test the trained model on 100 randomly sampled observed galaxies in the  $g$ ,  $r$ , and  $i$  bands (for 300 total image–profile pairs) drawn from the data set and which are set aside entirely during training. We use the model with the lowest validation loss; epoch 160.

We run an entirely automated inference on an Intel Xeon CPU E5-2650 v3 CPU at a rate of 0.9 galaxies per second.

Fig. 3 shows a random selection of 25 Pix2Prof inferred test set SB profiles superimposed on to the Courteau (1996) SB profiles. Since we have trained Pix2Prof to directly infer a SB profile from a galaxy image we do not produce intermediate steps (such as the galaxy centre, ellipticity profile, or position angle profile). However, one could estimate these values if Pix2Prof is explicitly trained to reproduce them. Fig. 4 shows the error distribution of the test set as well as the test set error per distance in physical units from the galaxy centre. We define error as the absolute of Fig. 3’s residual, the absolute deviation:

$$\eta = |y - p|, \quad (3)$$

where  $p$  is a prediction, and  $y$  is measured via Courteau (1996). The units of SB call for additional care in defining our errors. Since SB values are defined on a logarithmic scale, equation (3) is really a form of fractional error:

$$\eta = \left| 2.5 \log_{10} \frac{I_p}{C} - 2.5 \log_{10} \frac{I_y}{C} \right| = \left| -2.5 \log_{10} \frac{I_y}{I_p} \right|, \quad (4)$$

where  $C$  is a constant reference brightness.  $\{I_p, I_y\}$  are brightnesses in linear units.

We take the median of this error per galaxy profile to produce the violin plots in Fig. 4a, and we take the median of this error across profiles to produce the line plot in Fig. 4a. Fig. 4a’s line plot shows that the error increases with radius away from the galaxy centre towards regions containing less signal, as expected. We find that the median test set absolute deviation is  $0.41 \text{ mag arcsec}^{-2}$  with an interquartile range of  $0.21 \text{ mag arcsec}^{-2}$ . We also find that the median test set absolute deviation for  $y$  values brighter than the SDSS limiting SB ( $26.5 \text{ mag arcsec}^{-2}$ ) is  $0.34 \text{ mag arcsec}^{-2}$ , with an interquartile range of  $0.22 \text{ mag arcsec}^{-2}$ . Errors of this scale mean that profiles generated via Pix2Prof will be immediately useful for rough searches; it would be possible to categorise galaxies roughly by brightness, isophotal radius, scale length, and other structural parameters. Further refinement of the model may reduce error, enabling more sophisticated processing and analysis of generated SB profiles. Possible refinements are described in Section 4.

In Fig. 5, the three bands’ median errors are separated as a function of galactocentric radius. Close to the galaxy, there is little difference in the three bands’ median predictions. However, as we proceed outwards, the  $r$ -band’s error is higher than the  $g$ -band’s, and the  $i$ -band’s error is higher still. This is due to a difference in the instrumental noise between the three bands, as evidenced in the difference

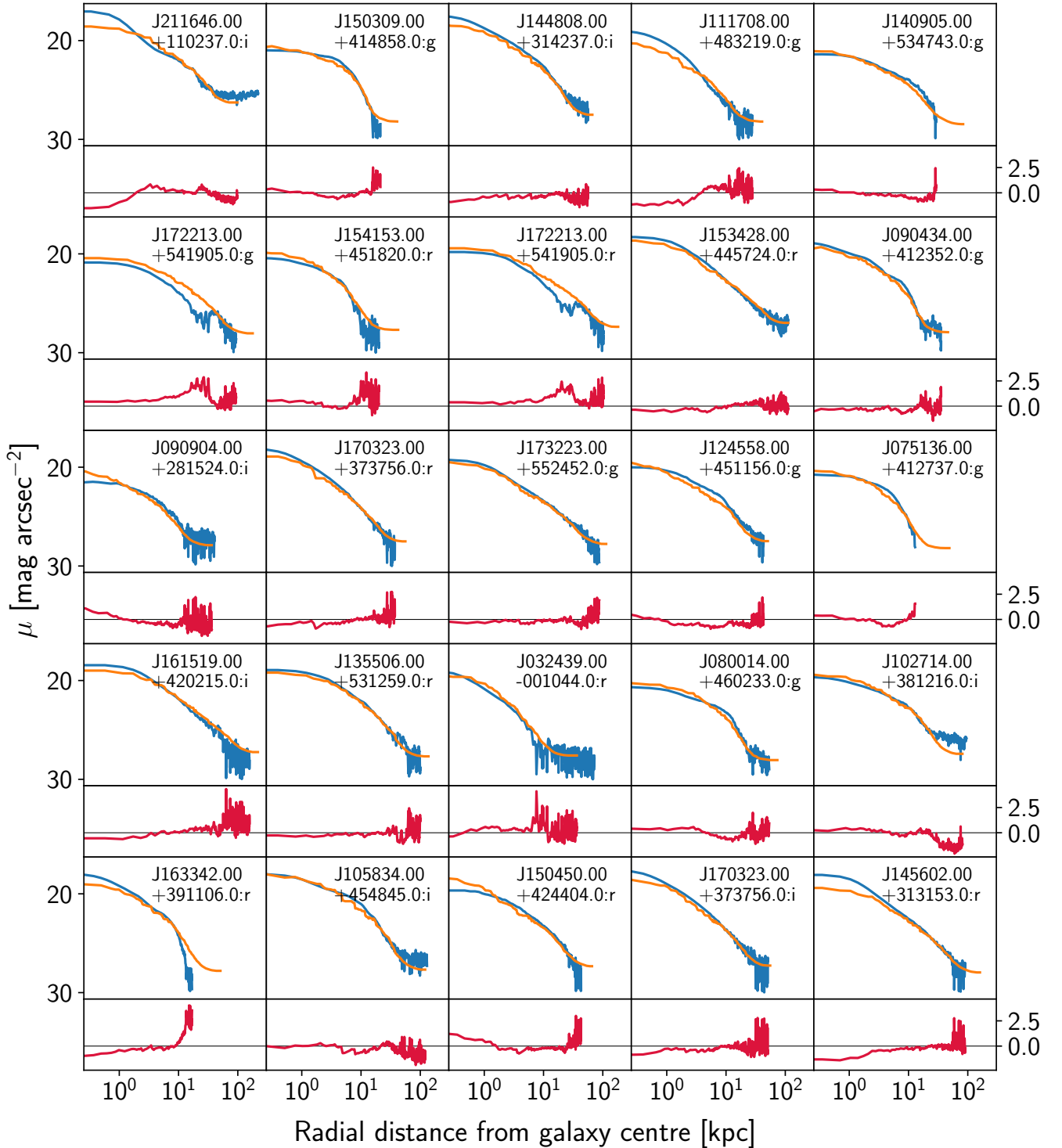
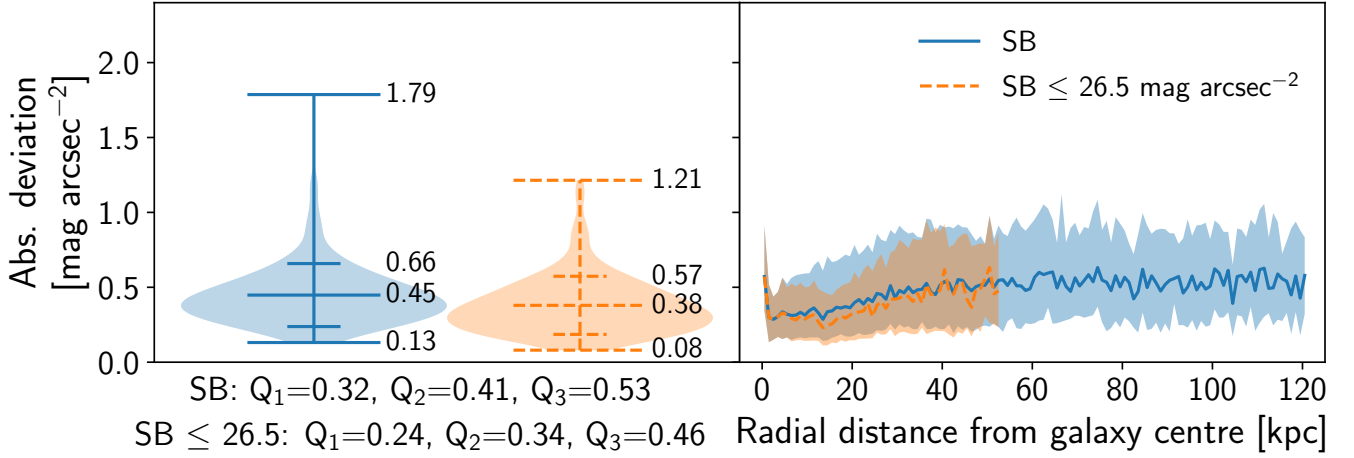
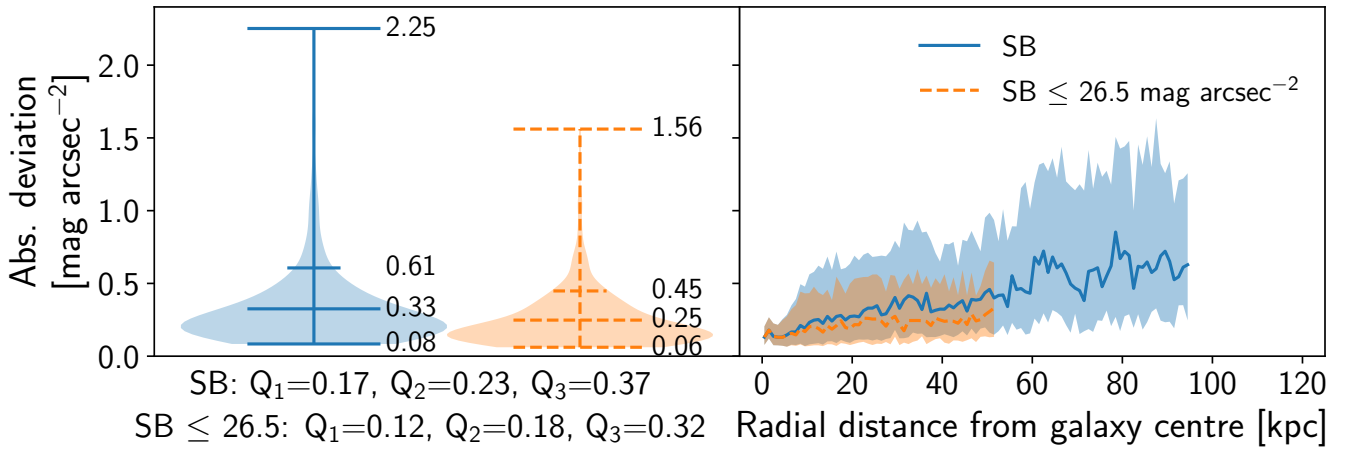


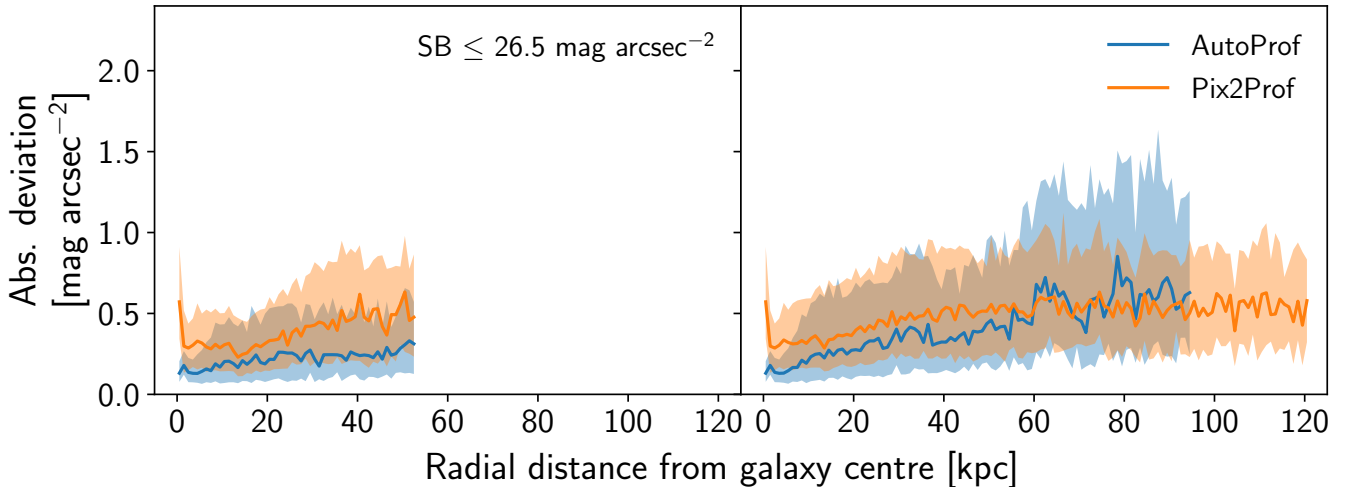
**Figure 3.** Randomly sampled test set predicted SB galaxy profiles (orange) superimposed onto SB profiles measured via the Courteau (1996) method (blue).  $\mu$  is the surface brightness. Distances from centre are in log scale to emphasise divergences in the high signal-to-noise ratio region closer to the galaxies' centres. Below each SB profile plot is the residual defined as  $res = y - p$ , where  $y$  is the profile as measured according to Section 2.1, and  $p$  is the prediction. The galaxies' J2000 celestial coordinates and spectral bands are indicated at the top right of each graph.



(a) Summary statistics for Pix2Prof.



(b) Summary statistics for AutoProf (see §3.1).



(c) Median error per kpc from galaxy centre comparison between Pix2Prof and AutoProf.

**Figure 4.** Approximation errors as defined in equation (3). Fig. 4a shows summary statistics for Pix2Prof. For comparison, Fig. 4b depicts the same statistics for AutoProf. In all of the above figures we define absolute deviation as relative to the Courteau (1996) test set profiles. The leftmost violin plot in Fig. 4a and 4b shows the distribution of median test set errors. The rightmost violin plot in Fig. 4a and 4b shows the same distribution for only SB values below the SDSS limiting SB of 26.5 mag arcsec<sup>-2</sup>. The maximum, minimum, mean, and (mean + standard deviation) are labelled. Below the violin plots are their distribution quartiles. The line plots show the median error per kpc from the galaxy centre, with the interquartile range shaded. To reduce the effect of small sample size variability, the line plots are terminated once 90 per cent of the SB profiles reach their galaxy’s extent. Fig. 4c compares on the same axes the median errors per kpc from the galaxy centre for Pix2Prof and AutoProf.

**Table 2.** Pix2Prof eliminates all interactive steps in the Courteau (1996) algorithm, alleviating subjectivity and accelerating inference significantly.

| Process                             | Automated in:    |           |
|-------------------------------------|------------------|-----------|
|                                     | Courteau (1996)? | Pix2Prof? |
| Identify galaxy centre              | No               | Yes       |
| Estimate & remove sky background    | Yes              | Yes       |
| Remove foreground objects           | No               | Yes       |
| Fit contours                        | Yes              | Yes       |
| Extend contours to galaxy outskirts | No               | Yes       |
| Smooth isophotes                    | Yes              | Yes       |
| Interpolate poorly fitted data      | No               | Yes       |

in the spectral bands’ median galaxy image signal-to-noise ratios:  $\text{SNR}_g = 41.6$ ;  $\text{SNR}_r = 35.8$ ;  $\text{SNR}_i = 28.4$ .

Fig. 6a shows each test set galaxy’s ellipticity against the galaxy profile’s median absolute deviation. The ellipticity is defined as the final isophote ellipticity for a profile calculated using the Courteau (1996) method. Fig. 6b shows each test set galaxy’s semimajor axis radius for the first isophote whose value is greater than or equal to  $23.5 \text{ mag arcsec}^{-2}$ . In both of these cases, we run a linear regression and find no significant correlation, suggesting that Pix2Prof’s predictions are equally robust when inferring across galaxies with a range of sizes and ellipticities.

Figs 3 and 4 show that Pix2Prof can successfully approximate a complicated astrophysical image processing pipeline with low deviation ( $0.34 \text{ mag arcsec}^{-2}$  averaged over the test set). Processing 0.9 galaxies per second on an Intel Xeon E5-2650 v3 CPU, Pix2Prof improves on the speed of the classical image analysis method of Courteau (1996) by more than two orders of magnitude. For comparison, an astronomer trained to use the Courteau (1996) method can typically process  $\sim 150$  galaxies in a full eight hour working day (or  $\sim 0.005$  galaxies per second). However, even astronomers must rest and so the true working rate for a human would be  $\sim 150$  galaxies per 24 hours, or  $\sim 0.002$  galaxies per second.

As Table 2 shows, Pix2Prof eliminates any manual interaction from SB profile inference, alleviating the issue of subjectivity in the different methods developed for such tasks; Pix2Prof will infer the same profile every time for a given galaxy image, whereas a human may not. The full automation of Pix2Prof enables a complete parallelisation, and thus significant gain in parallel throughput of galaxy profile estimation.

### 3.1 Comparison with AutoProf

AutoProf (Stone et al. 2021) is a sibling method to Pix2Prof that uses a more standard astronomical pipeline to tackle the problem of non-parametric automated SB profile inference. A combination of standard image analysis packages from PHOTUTILS (Bradley et al. 2019) and novel techniques are used to construct a robust isophotal pipeline. Initial image analysis such as determining the PSF, centre finding, star masking, and sky background subtraction are performed using PHOTUTILS. Next, AutoProf simultaneously fits an ellipticity and position angle profile by minimising low order FFT coefficients along each isophote plus a regularisation term (Shalev-Shwartz & Ben-David 2014). The regularisation term penalises neighbouring ellipticity and position angle values that deviate significantly, ultimately favouring smooth profiles. Once the profiles have converged, AutoProf extracts the median SB along each isophote and determines the error with a 68.3 per cent quartile range. A curve of growth is de-

termined by appropriately integrating the SB profile and propagating errors.

Fig. 4 compares the performance of Pix2Prof and AutoProf. AutoProf is found to produce SB profiles that are a slightly closer match to those produced via Courteau (1996) than Pix2Prof. The difference in absolute deviation between the two methods’ profiles is typically around  $0.1\text{--}0.2 \text{ mag arcsec}^{-2}$ . However, AutoProf’s accuracy comes with a time penalty; AutoProf takes on average 490 s to produce a profile on an Intel Xeon E5-2650 v3 CPU, a rate of 0.002 galaxies per second. This rate is roughly equivalent to the throughput of a human running the Courteau (1996) method. Pix2Prof processes 0.9 galaxies per second on the same hardware. Pix2Prof also offers more flexibility; it can be retrained to recreate any (semi) manual galaxy profile fitting pipeline and is therefore not limited to automation of the Courteau (1996) method.

AutoProf is presented in Stone et al. (2021), and its code is available at <https://github.com/ConnorStoneAstro/AutoProf>.

## 4 DISCUSSION AND CONCLUSIONS

While Pix2Prof can rapidly and accurately produce profiles of arbitrary length, there are some limitations to this technique. Principally, any profile produced will be biased to the training set. For instance, if Pix2Prof is trained on primarily nearby galaxies, it may not yield accurate profiles for more distant systems whose images will be poorly resolved. Similarly, if the model is trained on galaxy image–profile pairs as produced by numerical simulations the model will encode any flaws, incompleteness, or bias inherent to each simulation and will not encode instrumental effects (e.g. read-out noise) unless properly included. The same issue will occur if we train on galaxy image–profile pairs sampled from one survey and deploy the trained model on a dissimilar survey, for example SDSS, and LSST (York et al. 2000; Ivezić et al. 2019). It may be possible to mitigate this problem with an image domain translator (i.e. Zhu et al. 2017; Isola et al. 2017; Choi et al. 2018) that could transform observations so that they match a given survey. Of course, the Courteau (1996) measured profiles may also not entirely reflect the ‘true’ SB profile, due to modelling assumptions, human bias, and inherent noisiness in measurement. As neural networks typically require very large data sets, our relatively small data set is likely not reflecting the true potential of the model. Therefore, a larger set of training data could improve the results presented here. Generating a larger data set from simulated galaxies for training Pix2Prof will be a future project.

As described in Jia et al. (2015), due to the vanishing gradient problem a LSTM or GRU may ‘forget’ an image encoding as it unrolls. For Pix2Prof, this will manifest in a loss of accuracy at larger galactocentric radius. We see this effect in Fig. 4a’s line plot and Fig. 5, but we cannot disentangle the individual contributions from image noise and the model architecture. However, assuming that the noise is significantly caused by GRU ‘forgetfulness’, future Pix2Prof models could imitate Jia et al. (2015) and counteract the noise by reinjecting the image encoding into the GRU’s hidden state periodically as it unrolls. Another solution could involve adopting an architecture that suffers less from the vanishing gradient problem, such as the Transformer (Vaswani et al. 2017). The non-sequential nature of a Transformer would also allow us to parallelise output at inference time, reducing processing time even further.

In Section 1 we stressed the need for efficient and fully automated methods for timely analysis of ultra-large scale astrophysical imaging survey data. We believe that Pix2Prof addresses this challenge. Pix2Prof can predict any galaxy profile, given the right simulated

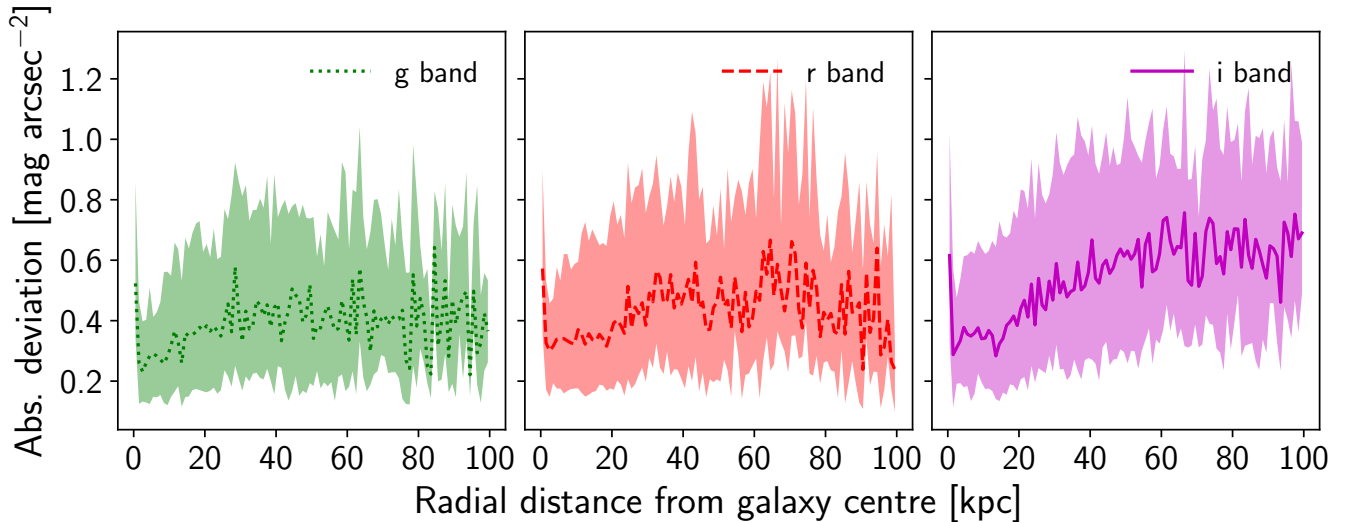


**Figure 5.** Median test set error per kpc from the galaxy centre, with the interquartile range shaded, split into the three bands present in the test set.

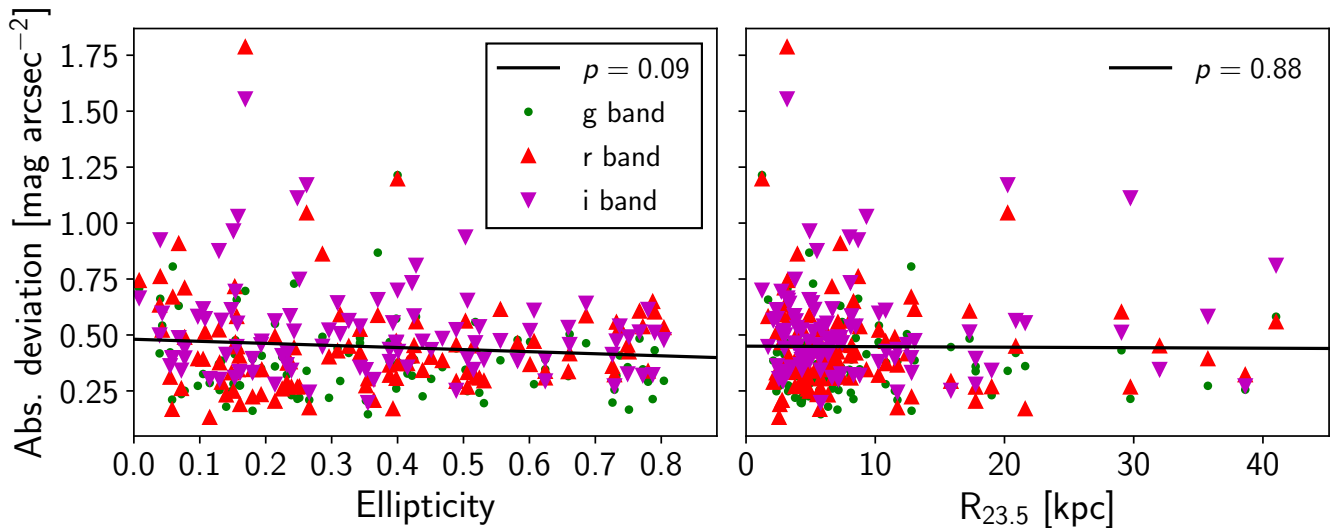


**Figure 6.** Median test set error over each galaxy predicted profile, plotted against each galaxy’s ellipticity (left, 6a), and size at  $R_{23.5}$  (right, 6b).  $p$  values obtained via a linear regression are stated in the legends.

or observed data set. Training Pix2Prof on simulated galaxy images offers additional benefits; the model could be trained on information that is only inferred indirectly in observations. For instance, Pix2Prof could train on sets of galaxy image–mass profile pairs directly in order to predict dark matter halo profiles, as mass profiles cannot be recovered classically by direct imaging observations. Furthermore, Pix2Prof has the potential to automate any galaxy profile fitting routine and be ported to other forms of galaxy image analysis that may not rely on isophotal analysis, but still produce a float sequence given a multidimensional array. These analyses could include galaxy component decompositions, the characterisation of galaxy interactions and distortions, pixelised stellar population synthesis, inference of galaxy mass distributions, and more (e.g. Eneev et al. 1973; Vazdekis 2001; Peng et al. 2002). In a future paper, we will demonstrate how Pix2Prof can be used to recover simultaneously the galaxy SB profile as well as the ellipticity profile and curve of growth of a galaxy.

An exciting future investigation involves building a system that can predict properties of unseen classes of objects. This could be achieved by building up a ‘prior’ that encodes known objects into a latent space and interpolates between their latent spatial representations at inference time. A generative model like the Generative Adversarial Network (GAN; Goodfellow et al. 2014) or Variational Autoencoder (VAE; Kingma & Welling 2013) could achieve this (i.e. Spindler et al. 2020). Such a model could quickly identify astrophysically ‘interesting’ objects in a large field survey. The ability to search for rare objects in large unstructured data sets will become increasingly more important as new large scale astronomical surveys come online (Chambers et al. 2016; Aihara et al. 2017; Ivezić et al. 2019).

In summary, we have introduced a fully automated deep learning model for the extraction of sequential data from galaxy imagery. We have tested this model by applying it to the specific problem of estimating galaxy SB profiles, a process that previously required



manual, time-consuming human intervention. We have tested our model on unseen galaxy images and found that our model has an average absolute deviation of  $0.34 \text{ mag arcsec}^{-2}$  with an interquartile range of  $0.22 \text{ mag arcsec}^{-2}$ , while inferring SB profiles over two orders of magnitude faster than the classic (interactive) algorithm it automates.

## DATA AND CODE AVAILABILITY

The code and trained model used in this paper is available at <https://github.com/Smith42/pix2prof>. The profile data set used to train the network will be released separately (Arora et al., in preparation).

## CARBON EMISSIONS

The training of deep learning models requires considerable energy, contributing to carbon emission and therefore climate change (Strubell et al. 2019; Lacoste et al. 2019). The energy used while training Pix2Prof on a single NVIDIA V100 GPU is estimated to be  $\sim 20 \text{ kWh}$  ( $5.54 \text{ kg CO}_2 \text{ eq}$ ) according to the Machine Learning Impact calculator described in Lacoste et al. (2019). This is equivalent to driving 28 miles in a typical European passenger car<sup>1</sup>. To counteract further emission from redundant retraining, we follow the recommendations of Strubell et al. (2019) and make available the fully trained model, as well as the code to run it. Also, we will make available trained models for any improvements that we make to Pix2Prof in the future.

## ACKNOWLEDGEMENTS

This research made use of the University of Hertfordshire's High Performance Computing facility (<http://uhhpc.herts.ac.uk/>). We are grateful to the Natural Sciences and Engineering Research Council of Canada, the Ontario Government, Queen's University, and the Royal Society for critical support through various scholarships and grants. M.J.S. thanks Queen's University and the research group of Stéphane Courteau for their support and hospitality in 2019 while this paper was conceived and developed. We also thank reviewers at the NeurIPS 2020 conference, as well as the MNRAS editor and referee for helpful comments and suggestions. The galaxy icon in Fig. 2 is by Agata Kuczmirska and is available under the CC-BY-4.0 licence at <https://goodstuffnononsense.com/hand-drawn-icons/space-icons/>.

## REFERENCES

Ahn C. P., et al., 2014, *ApJS*, 211, 17  
 Ahumada R., et al., 2020, *ApJS*, 249, 3  
 Aihara H., et al., 2017, *PASJ*, 70, S4  
 Aihara H., et al., 2019, *PASJ*, 71, 114  
 Bell E. F., McIntosh D. H., Katz N., Weinberg M. D., 2003, *ApJS*, 149, 289  
 Bernardi M., Sheth R. K., Nichol R. C., Schneider D. P., Brinkmann J., 2005, *AJ*, 129, 61

Blanton M. R., Lupton R. H., Schlegel D. J., Strauss M. A., Brinkmann J., Fukugita M., Loveday J., 2005, *ApJ*, 631, 208  
 Bradley L., et al., 2019, *Astropy/photutils*: v0.6  
 Brinchmann J., Charlot S., White S. D. M., Tremonti C., Kauffmann G., Heckman T., Brinkmann J., 2004, *MNRAS*, 351, 1151  
 Chambers K. C., et al., 2016, preprint ([arXiv:1612.05560](https://arxiv.org/abs/1612.05560))  
 Cho K., van Merriënboer B., Gülçehre Ç., Bahdanau D., Bougares F., Schwenk H., Bengio Y., 2014, in Moschitti A., Pang B., Daelemans W., eds, Proceedings of EMNLP 2014. ACL, p. 1724 ([arXiv:1406.1078](https://arxiv.org/abs/1406.1078))  
 Choi Y., Choi M., Kim M., Ha J., Kim S., Choo J., 2018, in Proceedings of CVPR 2018. IEEE Computer Society, p. 8789 ([arXiv:1711.09020](https://arxiv.org/abs/1711.09020))  
 Courteau S., 1996, *ApJS*, 103, 363  
 Eisenstein D. J., et al., 2011, *AJ*, 142, 72  
 Eneev T. M., Kozlov N. N., Sunyaev R. A., 1973, *A&A*, 22, 41  
 Fernández Lorenzo M., Sulentic J., Verdes-Montenegro L., Argudo-Fernández M., 2013, *MNRAS*, 434, 325  
 Fukushima K., 1980, *Biol. Cybern.*, 36, 193  
 Gilhuly C., Courteau S., 2018, *MNRAS*, 477, 845  
 Glorot X., Bordes A., Bengio Y., 2011, in Gordon G., Dunson D., Dudík M., eds, Proceedings of Machine Learning Research Vol. 15, Proceedings of the Fourteenth International Conference on Artificial Intelligence and Statistics. Proceedings of Machine Learning Research, Fort Lauderdale, FL, USA, p. 315, <http://proceedings.mlr.press/v15/glorot11a.html>  
 Goodfellow I., Pouget-Abadie J., Mirza M., Xu B., Warde-Farley D., Ozair S., Courville A., Bengio Y., 2014, in Ghahramani Z., Welling M., Cortes C., Lawrence N. D., Weinberger K. Q., eds, Proceedings of NIPS 27. Curran Associates, Inc., <http://papers.nips.cc/paper/5423-generative-adversarial-nets.pdf>  
 Hall M., Courteau S., Dutton A. A., McDonald M., Zhu Y., 2012, *MNRAS*, 425, 2741  
 He K., Zhang X., Ren S., Sun J., 2016, in Proceedings of CVPR 2016. IEEE Computer Society, p. 770 ([arXiv:1512.03385](https://arxiv.org/abs/1512.03385))  
 Hochreiter S., Schmidhuber J., 1997, *Neural Comput.*, 9, 1735  
 Hossain M. Z., Sohel F., Shiratuddin M. F., Laga H., 2019, *ACM Comput. Surv.*, 51, 118  
 Isola P., Zhu J.-Y., Zhou T., Efros A. A., 2017, in Proceedings of CVPR 2017. IEEE Computer Society, p. 5967 ([arXiv:1611.07004](https://arxiv.org/abs/1611.07004))  
 Ivezić Ž., et al., 2019, *ApJ*, 873, 111  
 Jedrzejewski R. I., 1987, *MNRAS*, 226, 747  
 Jia X., Gavves E., Fernando B., Tuytelaars T., 2015, in Proceedings of ICCV 2015. IEEE Computer Society, p. 2407 ([arXiv:1509.04942](https://arxiv.org/abs/1509.04942))  
 Kingma D. P., Ba J., 2014, preprint, ([arXiv:1412.6980](https://arxiv.org/abs/1412.6980))  
 Kingma D. P., Welling M., 2013, preprint, ([arXiv:1312.6114](https://arxiv.org/abs/1312.6114))  
 Lacoste A., Luccioni A., Schmidt V., Dandres T., 2019, preprint, ([arXiv:1910.09700](https://arxiv.org/abs/1910.09700))  
 LeCun Y., Boser B., Denker J. S., Henderson D., Howard R. E., Hubbard W., Jackel L. D., 1989, *Neural Comput.*, 1, 541  
 Paszke A., et al., 2019, in Wallach H., Larochelle H., Beygelzimer A., d Alché-Buc F., Fox E., Garnett R., eds, Proceedings of NIPS 32. Curran Associates, Inc., <http://papers.neurips.cc/paper/9015-pytorch-an-imperative-style-high-performance-deep-learning-library.pdf>  
 Peng C. Y., Ho L. C., Impy C. D., Rix H.-W., 2002, *AJ*, 124, 266  
 Robbins H., Monro S., 1951, *Ann. Math. Stat.*, 22, 400  
 Shalev-Shwartz S., Ben-David S., 2014, Understanding machine learning: From theory to algorithms. Cambridge university press  
 Shen S., Mo H. J., White S. D. M., Blanton M. R., Kauffmann G., Voges W., Brinkmann J., Csabai I., 2003, *MNRAS*, 343, 978  
 Spindler A., Geach J. E., Smith M. J., 2020, *MNRAS*, 502, 985  
 Srivastava N., Hinton G., Krizhevsky A., Sutskever I., Salakhutdinov R., 2014, *JMLR*, 15, 1929  
 Srivastava R. K., Greff K., Schmidhuber J., 2015, in Cortes C., Lawrence N., Lee D., Sugiyama M., Garnett R., eds, Proceedings of NIPS 28. Curran Associates, Inc., <https://proceedings.neurips.cc/paper/2015/file/215a71a12769b056c3c32e7299f1c5ed-Paper.pdf> ([arXiv:2104.07034](https://arxiv.org/abs/2104.07034))  
 Stone C., Courteau S., Arora N., 2021, preprint ([arXiv:2104.07034](https://arxiv.org/abs/2104.07034))  
 Strom S. E., Strom K. M., Goad J. W., Vrba F. J., Rice W., 1976, *ApJ*, 204,

<sup>1</sup> According to the European Environmental Agency: <https://www.eea.europa.eu/highlights/average-co2-emissions-from-new-cars-vans-2019>

684

- Strubell E., Ganesh A., McCallum A., 2019, in Proceedings of ACL 57. Association for Computational Linguistics, Florence, Italy, p. 3645, [doi:10.18653/v1/P19-1355](https://doi.org/10.18653/v1/P19-1355)
- Sutskever I., Vinyals O., Le Q. V., 2014, in Ghahramani Z., Welling M., Cortes C., Lawrence N., Weinberger K. Q., eds, Proceedings of NIPS 27. Curran Associates, Inc., <https://proceedings.neurips.cc/paper/2014/file/a14ac55a4f27472c5d894ec1c3c743d2-Paper.pdf>
- Trujillo I., Chamba N., Knapen J. H., 2020, *MNRAS*, 493, 87
- Tuccillo D., Huertas-Company M., Decenci ere E., Velasco-Forero S., Dom inguez S anchez H., et al., 2018, *MNRAS*, 475, 894
- Vaswani A., Shazeer N., Parmar N., Uszkoreit J., Jones L., Gomez A. N., Kaiser Ł., Polosukhin I., 2017, in Guyon I., Luxburg U. V., Bengio S., Wallach H., Fergus R., Vishwanathan S., Garnett R., eds, Proceedings of NIPS 30. Curran Associates, Inc., <https://proceedings.neurips.cc/paper/2017/file/3f5ee243547dee91fbd053c1c4a845aa-Paper.pdf>
- Vazdekis A., 2001, *Ap&SS*, 276, 921
- Vinyals O., Toshev A., Bengio S., Erhan D., 2015, in Proceedings of CVPR 2015. IEEE Computer Society, p. 3156 ([arXiv:1411.4555](https://arxiv.org/abs/1411.4555))
- Wang C., Yang H., Bartz C., Meinel C., 2016, in Proceedings of the 24th ACM International Conference on Multimedia. ACM, p. 988 ([arXiv:1604.00790](https://arxiv.org/abs/1604.00790))
- Xu K., Ba J. L., Kiros R., Cho K., Courville A., Salakhutdinov R., Zemel R. S., Bengio Y., 2015, in Proceedings of ICML 32. p. 2048 ([arXiv:1502.03044](https://arxiv.org/abs/1502.03044))
- York D. G., et al., 2000, *AJ*, 120, 1579
- Zhu J., Park T., Isola P., Efros A. A., 2017, in Proceedings of ICCV 2017. IEEE Computer Society, p. 2242 ([arXiv:1703.10593](https://arxiv.org/abs/1703.10593))

This paper has been typeset from a  $\text{\TeX}/\text{\LaTeX}$  file prepared by the author.